Optimized Method of Lines for non-linear waveguide problems

Waldemar Spiller (walspill@yahoo.de)
FernUniversitat in Hagen https://orcid.org/0000-0001-6365-4958

Research Article

Keywords: Method of lines (MoL), non-linear generalized transmission line equations, impedance/admittance transformation, finite differences, non-linear waveguides, second-order non-linear phenomena, self-consistent solutions

Posted Date: February 9th, 2022

DOI: https://doi.org/10.21203/rs.3.rs-1326606/v1

Optical and Quantum Electronics manuscript No.
(will be inserted by the editor)

Optimized Method of Lines for non-linear waveguide problems

Waldemar Spiller

Received: date / Accepted: date

Abstract The Method of Lines is a semi-analytical versatile tool for the solution of partial differential equations. For the analysis of spatial complex linear waveguide structures, this method is combined with impedance/admittance and field transformation, as well as with finite differences. This paper extends this approach to the treatment of structures with non-linear dielectric materials. The non-linear generalized transmission line equations are derived. An iterative algorithm based on the impedance/admittance transformation with the field transformation obtains efficient and self-consistent solutions. The specific limiting factors for the algorithm and how to overcome them were investigated. A bidirectional, spatially, and temporally periodic energy exchange between the harmonics were found. For demonstration, a stripe waveguide with the non-linear core is considered. The Kerr non-linearity was investigated, though the general case is treatable. The approach can be used for any spatial structure, including, for instance, photonic crystal waveguides and metamaterials.

Keywords Method of lines (MoL), non-linear generalized transmission line equations, impedance/admittance transformation, finite differences, non-linear waveguides, second-order non-linear phenomena, self-consistent solutions

1 Introduction

The Method of Lines (MoL) in combination with impedance/admittance and field transformation (IAFT) is used to analyze electromagnetic waves, (Helfert and Pregla, 2002), (Pregla and Helfert, 2002), (Helfert et al, 2003), (Pregla, 2008). The use cases are linear waveguiding structures of microwave technology and optics. The core of the theory is the solution of generalized transmission line equations (GTL). The GTL equations describe the relationship between the transverse components of the electric and the magnetic field. The GTL equations are derived from Maxwell's equations with specific boundary conditions for a specific structure. In the case of complex structures, a combination with finite differences (FD) can be used, (Helfert and Pregla, 1996). The conventional procedure is as follows: The calculation area is covered with lines. The model of a structure is divided into homogeneous sections in the direction of the analytical solution. For most practical cases, the discretization of the coordinates perpendicular to the direction of propagation is assumed to be favorable. For example, the cross-section of a structure is discretized, and the analytical solution is used in the direction of propagation. In the case of the application of the FD, the structure is divided into sufficiently short sections. These sections can be assumed to be homogeneous. Their length is set equal to the step length of the FD. A corresponding interpolation between the points of the FD is important for the efficiency and adequacy of the solution. The discretized GTL equations in matrix form are solved analytically for each homogeneous section (or for each step of the FD). The GTL matrices consist of differential operator matrices with corresponding boundary conditions and material parameters. The materials have so far been assumed to be linear. To determine the field distributions, the solution for the entire structure is usually performed in two procedures: First, an impedance/admittance transformation takes place, and then the field transformation.

The impedance/admittance transformation serves to determine all two-port network parameters of all sections and thus also their respective loads. Because the structure consists of different homogeneous sections, the tangential field components have to be matched at interfaces. The impedance/admittance transformation is one such matching over the sections. The two-port network parameters of the sections can be calculated from the conditions

W. Spiller, E-mail: walspill@yahoo.de

for open circuit and short circuit set at the output of the structure. The calculation of the impedance/admittance transformation is done step by step, i.e., section by section, mostly in the direction from the output of the structure to the input. The field transformation serves to determine the electric and magnetic fields on each homogeneous section or (which is identical) in each step of the FD. The procedure is possible if the impedances and/or admittances of all sections (or all FD steps) have already been calculated during the previous run of the impedance/admittance transformation.

The field transformation is also performed recursively, section by section, mostly from the input to the output of the structure, through all sections. The start value of the field at the input of the structure is specified. It can be, i.e., a Floquet fundamental mode transformed into the original domain. The introductory representation of the GTL, e.g., the tensor of the material parameters and normalization, is contained in (Pregla, 2006-a) or (Pregla, 2006-b). A comprehensive treatment of the MoL for the analysis of electromagnetic waves, i.e., various discretization schemes and boundary conditions, linear GTL equations, impedance/admittance, and field transformation, their combination with the FD, periodic problems, and the application for concrete structures is contained in the monograph (Pregla, 2008).

Generally speaking, all materials are non-linear. When dealing with stronger electromagnetic fields, the non-linearity can no longer be neglected. More so, the non-linearity is seen as a new tool to be used, (Gomez-Ullate et al., 2010), (Agrawal, 2007), (Boyd and Fischer, 2001), (Boyd, 2020), (Knyazyan, Pregla, and Helfert, 2004). A suitable example is the second harmonic generation (SHG). The MoL (or MoL-IAFT-FD) has its characteristic properties, which are particularly interesting for the analysis of non-linear waveguide phenomena: lower computation time compared to the fully numerical methods, stationary behavior, no phenomenon of relative convergence, very accurate calculation of the field distribution because of the relation to the Discrete Fourier Transformation, no spurious modes, etc., (Pregla, 2008), (Jamid and Akram, 2002). The following questions arise: How should the non-linear problem be described? Which solutions are possible? What are the limiting factors of the solution? How can the limiting factors be overcome? Is further research in this direction worthwhile?

The first possible description is non-linear generalized transmission line equations (NGTL). These will be derived from Maxwell's equations, taking into account the polarization of the medium. The NGTL equations are the coupled differential equations of the 1-st order. However, here's to do with non-linear processes: The result of the calculation - e.g., a spatial electric field distribution for each FD step - depends in principle on "itself". According to (Hermann and Saravi, 2016), it is hypothesized that the equations have one and non-singular solutions. This is finally confirmed by means of an iterative algorithm with a self-consistent, convergent solution. The length of the non-linear part of the structure (interaction length) turned out to be the first limiting factor of the numerical solution. Here, the required accuracy of the calculation and the numerical effort should be weighed for each specific application. It has been found that a suitable way of interpolating the FD steps can significantly overcome this limit: Instead of the linear and quadratic interpolation already established in (Pregla, 2006-a) and (Pregla, 2006-b), the use of the one-step methods of the 4th order enabled the analysis of a structure up to 25 times longer.

The paper is organized as follows: The NGTL equations are derived in section 2. Here a scheme is followed that was presented earlier by (Knyazyan, Pregla, and Helfert, 2004). Section 3 represents the aspects of the discretization and the SHG. The numerical solution mechanism and the specific numerical problems are presented in section 4. The verification of numerical results can be found in section 5. The conclusions are presented in section 6. The appendix contains an auxiliary derivation.

2 Basic formulas

This section introduces non-linearity. It is started with time-dependent Maxwell's curl equations, (Saleh and Teich, 2007), which are given by

$$\nabla\times \vec{e} = -\mu_0 \frac{\partial \vec{h}}{\partial t} \qquad \nabla\times \vec{h} = \varepsilon_0 \frac{\partial \vec{e}}{\partial t} + \frac{\partial \vec{P}}{\partial t} \tag{1}$$

The polarization dipole moment per unit volume, or polarization $\vec{P}\,(t)$ of a material system can be described as a power series in the field strength $\vec{e}\,(t)$, according to, e.g., (Boyd, 2020):

$$\vec{P}\,(t) = \varepsilon_0 \left(\chi\, \vec{e}\,(t) + \chi_2 e^2(t)\, \vec{a}_e + \chi_3 e^3(t)\, \vec{a}_e + ... \right) \tag{2}$$

where $\vec{e}\,(t) = e(t)\, \vec{a}_e$ and $\vec{a}_e$ being the unit vector in the direction of electric field $\vec{e}$. Here χ is known as the susceptibility and ε_0 is the permittivity of free space. Further on in the paper, a number as a subscript of a quantity

denotes the number of the harmonics of the fundamental frequency ω, i.e., the susceptibility or the complex amplitude of the electric field for the frequency 2ω, χ_2 and E_2, respectively. Quantities without a subscript or with subscript 1 correspond to the fundamental frequency, i.e., χ.

So, following (Boyd, 2020), the polarization vector $\vec{P}$ can be divided into two parts, a linear and a non-linear, $\vec{P}(t) = \vec{P}_{\mathrm{L}}(t) + \vec{P}_{\mathrm{NL}}(t)$. In the paper the non-linear part $\vec{P}_{\mathrm{NL}}$ of second order is assumed.

$$\vec{P} = \varepsilon_0 \left(\chi \vec{e} + \chi_2 e^2 \vec{a}_e \right) \qquad \vec{P}_{\mathrm{NL}} = \varepsilon_0 \chi_2 e^2 \vec{a}_e \tag{3}$$

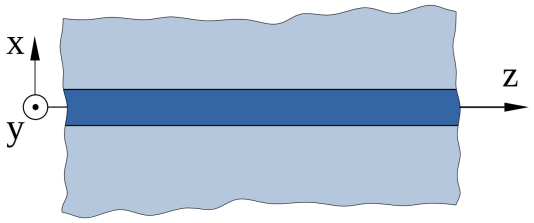

Fig. 1 2D-structure to be investigated (according to R. Pregla, 2014).

The propagation of TE modes with the components E_y, H_x, H_z (complex amplitudes) in the 2D-structure of Fig. 1 is investigated. For this purpose, wave equations corresponding to the application are derived. Thus, the general equations (1) with consideration of the model conditions in Fig. 1 reduces to

$$\frac{\partial e_y}{\partial z} = \mu_0 \frac{\partial h_x}{\partial t} \qquad \frac{\partial e_y}{\partial x} = -\mu_0 \frac{\partial h_z}{\partial t} \tag{4}$$

$$\frac{\partial h_x}{\partial z} = \varepsilon_0 \frac{\partial e_y}{\partial t} + \frac{\partial P_y}{\partial t} + \frac{\partial h_z}{\partial x} \tag{5}$$

The subscripts x, y, and z identify the corresponding projections on the coordinate axes. After differentiation of the eq. (5) with respect to the time and substituting eq. (4b) and P_y from eq. (3a) is obtained

$$\frac{\partial}{\partial z}\left(\frac{\partial h_x}{\partial t} \right) = \varepsilon_0 \varepsilon_r \frac{\partial^2 e_y}{\partial t^2} + \varepsilon_0 \chi_2 \frac{\partial^2 e_y^2}{\partial t^2} - \mu_0^{-1} \frac{\partial^2 e_y}{\partial x^2} \tag{6}$$

Introducing eq. (4a) into eq. (6) one obtains the wave equation for the model in Fig. 1

$$\frac{\partial^2 e_y}{\partial z^2} + \frac{\partial^2 e_y}{\partial x^2} - \varepsilon_0 \mu_0 \left(\varepsilon_r \frac{\partial^2 e_y}{\partial t^2} + \chi_2 \frac{\partial^2 e_y^2}{\partial t^2} \right) = 0 \tag{7}$$

2.1 Second harmonic generation

The complex functions of the field components are assumed, $(u = x, z)$:

$$\widetilde{H}_u = \widetilde{H}_{u1} e^{\mathrm{j}\omega t} + \widetilde{H}_{u2} e^{\mathrm{j}2\omega t} \qquad \widetilde{H}_u = \eta_0 H_u \tag{8}$$

$$E_y = E_1 e^{\mathrm{j}\omega t} + E_2 e^{\mathrm{j}2\omega t} \tag{9}$$

The subscripts "u1" and "u2" identify the corresponding components of the harmonics ("1" denotes the fundamental frequency ω); ε_0 and μ_0 are the vacuum permittivity and the magnetic permeability of free space. The magnetic field is normalized with the wave impedance in vacuum $\eta_0 = \sqrt{\mu_0/\varepsilon_0}$, thus, $\widetilde{H}_u = \eta_0 H_u$.
The complex function of the quadratic term can be described by (see appendix A1)

$$E_y^2 = E_1^* E_2 e^{\mathrm{j}\omega t} + \frac{1}{2} E_1^2 e^{\mathrm{j}2\omega t} \tag{10}$$

Where "*" denotes a complex conjugate. For the second derivative with respect to time, one obtains

$$\frac{\partial E_y^2}{\partial t} = \mathrm{j}\omega \left(E_1^* E_2 e^{\mathrm{j}\omega t} + E_1^2 e^{\mathrm{j}2\omega t} \right) \tag{11}$$

The complex functions will now be introduced into eq. (4) – (5) and normalize according to $\overline{z} = k_0 z, \overline{x} = k_0 x$ with $k_0 = \omega/v$ and $v = 1/\sqrt{\mu_0 \varepsilon_0}$.
Instead of the eqs. (4a) and (5) one obtains

$$\frac{\partial E_y}{\partial \overline{z}} = \mathrm{j}\widetilde{H}_{x1} e^{\mathrm{j}\omega t} + j2\widetilde{H}_{x2} e^{\mathrm{j}2\omega t} \tag{12}$$

$$\frac{\partial \widetilde{H}_x}{\partial \overline{z}} = \mathrm{j}\varepsilon_{r1} E_1 e^{\mathrm{j}\omega t} + 2\mathrm{j}\varepsilon_{r2} E_2 e^{\mathrm{j}2\omega t} + j\chi_{21} E_1^* E_2 e^{\mathrm{j}\omega t} + j\chi_{22} E_1^2 e^{\mathrm{j}2\omega t} + \frac{\partial \widetilde{H}_z}{\partial \overline{x}} \tag{13}$$

Instead of the eq. (4b) one obtains

$$\frac{\partial E_1}{\partial \overline{x}} = -\mathrm{j}\widetilde{H}_{z1} \qquad \frac{\partial E_2}{\partial \overline{x}} = -\mathrm{j}2\widetilde{H}_{z2} \tag{14}$$

The parts with $e^{\mathrm{j}\omega t}$ and $e^{\mathrm{j}2\omega t}$ are separated and one obtains

$$\frac{\partial E_1}{\partial \overline{z}} = \mathrm{j}\widetilde{H}_{x1} \qquad \frac{\partial \widetilde{H}_{x1}}{\partial \overline{z}} = \mathrm{j}\varepsilon_{r1} E_1 + \mathrm{j}\frac{\partial^2 E_1}{\partial \overline{x}^2} + \mathrm{j}\chi_{21} E_1^* E_2 \tag{15}$$

$$\frac{\partial E_2}{\partial \overline{z}} = \mathrm{j}2\widetilde{H}_{x2} \qquad \frac{\partial \widetilde{H}_{x2}}{\partial \overline{z}} = \mathrm{j}2\varepsilon_{r2} E_2 + \mathrm{j}\frac{1}{2}\frac{\partial^2 E_2}{\partial \overline{x}^2} + \mathrm{j}\chi_{22} E_1^2 \tag{16}$$

Introducing left eqs. (15) and (16) into right eqs. (15) and (16), respectively, one obtains the following coupled wave equations

$$\frac{\partial^2 E_1}{\partial \overline{z}^2} + \frac{\partial^2 E_1}{\partial \overline{x}^2} + \varepsilon_{r1} E_1 + \chi_{21} E_1^* E_2 = 0 \quad \frac{\partial^2 E_2}{\partial \overline{z}^2} + \frac{\partial^2 E_2}{\partial \overline{x}^2} + 4\varepsilon_{r2} E_2 + 2\chi_{22} E_1 E_1 = 0 \tag{17}$$

or introducing the difference operator $D_{\overline{x}\overline{x}} = \partial^2/\partial \overline{x}^2$

$$\frac{\partial^2}{\partial \overline{z}^2}\begin{bmatrix} E_1 \\ E_2 \end{bmatrix} + \begin{bmatrix} \varepsilon_{r1} + D_{\overline{x}\overline{x}} & \chi_{21} E_1^* \\ 2\chi_{22} E_1 & 4\varepsilon_{r2} + D_{\overline{x}\overline{x}} \end{bmatrix}\begin{bmatrix} E_1 \\ E_2 \end{bmatrix} = 0 \tag{18}$$

2.2 Equations for the general case

As shown in appendix A1, let us introduce the following notations

$$\begin{aligned} \widetilde{H}_u &= \sum_m \widetilde{H}_{um} e^{\mathrm{j}m\omega t}; \qquad u = x, z \\ E_y &= \sum_m E_m e^{\mathrm{j}m\omega t} \\ E_y^q &= \sum_m E_{ym}^q e^{\mathrm{j}m\omega t} \longrightarrow \frac{\partial E_y^q}{\partial t} = \mathrm{j}\omega \sum_m m E_{ym}^q e^{\mathrm{j}m\omega t} \end{aligned} \tag{19}$$

with $m = 1, 2, 3, ...$ Instead of eqs. (4) (left) and (5) one obtains

$$\frac{\partial E_m}{\partial \overline{z}} = \mathrm{j}m\widetilde{H}_{xm} = -\mathrm{j}m\Big(-\widetilde{H}_{xm}\Big) \tag{20}$$

$$\frac{\partial \widetilde{H}_{xm}}{\partial \overline{z}} = \mathrm{j}m\varepsilon_{rm} E_m + \mathrm{j}m\chi_{2m} E_{ym}^q + \frac{\partial \widetilde{H}_{zm}}{\partial \overline{x}} \tag{21}$$

Instead of eq. (4b) one obtains

$$\frac{\partial E_m}{\partial \overline{x}} = -\mathrm{j}m\widetilde{H}_{zm} \longrightarrow \frac{\partial \widetilde{H}_{zm}}{\partial \overline{x}} = \mathrm{j}m^{-1}\frac{\partial^2 E_m}{\partial \overline{x}^2} \tag{22}$$

Substituting eq. (22) into eq. (21) results in

$$\frac{\partial E_m}{\partial \overline{z}} = \mathrm{j}m\widetilde{H}_{xm} \qquad \frac{\partial \widetilde{H}_{xm}}{\partial \overline{z}} = \mathrm{j}m\varepsilon_{rm} E_m + \mathrm{j}m\chi_{2m} E_{ym}^q + \mathrm{j}m^{-1}\frac{\partial^2 E_m}{\partial \overline{x}^2} \tag{23}$$

As wave equation, one now obtains

$$\frac{\partial^2 E_m}{\partial \overline{z}^2} + \frac{\partial^2 E_m}{\partial \overline{x}^2} + m^2\varepsilon_{rm} E_m + m^2\chi_{2m} E_{ym}^q = 0 \tag{24}$$

Because E_{ym}^q is a function of $E_1, E_2, ...$ the wave equations are coupled. Frequencies from ω until 4ω are taken into account

$$\frac{\mathrm{d}^2}{\mathrm{d}\overline{z}^2}\begin{bmatrix} E_1 \\ E_2 \\ E_3 \\ E_4 \end{bmatrix} + \begin{bmatrix} \varepsilon_{r1} + D_{\overline{x}\overline{x}} & \chi_{21} E_1^* & \chi_{21} E_2^* & \chi_{21} E_3^* \\ 2\chi_{22} E_1 & 4\varepsilon_{r2} + D_{\overline{x}\overline{x}} & 4\chi_{22} E_1^* & 4\chi_{22} E_2^* \\ - & 9\chi_{23} E_1 & 9\varepsilon_{r3} + D_{\overline{x}\overline{x}} & 9\chi_{23} E_1^* \\ - & 8\chi_{24} E_2 & 16\chi_{24} E_1 & 16\varepsilon_{r4} + D_{\overline{x}\overline{x}} \end{bmatrix}\begin{bmatrix} E_1 \\ E_2 \\ E_3 \\ E_4 \end{bmatrix} = 0 \tag{25}$$

3 SHG with non-linear transmission line equations

An isotropy of the materials was assumed. The H- and E field components are discretized on two H and E line systems that are shifted from one another to a discretization distance across the direction of propagation z. The discretized field components are collected in vectors $\widehat{\mathbf{E}}$ and $\widehat{\mathbf{H}}$, corresponding to the spatial distribution of the complex amplitudes of the respective cross-section (a step of the FD). The electric and magnetic fields are calculated on two adjacent lines. For details, see in (Pregla, 2008), p. 15. The analytical solution is performed in the z-direction, whereby the TM and the TE polarization can be analyzed. The following definitions are introduced:

$$\widehat{\mathbf{E}} = \left[\widehat{\mathbf{E}}_1^t, \widehat{\mathbf{E}}_2^t\right]^{\mathrm{t}} \qquad \widehat{\mathbf{H}} = \left[-\widehat{\mathbf{H}}_{\mathrm{x1}}^t, -\widehat{\mathbf{H}}_{\mathrm{x2}}^t\right]^{\mathrm{t}} \tag{26}$$

In order to avoid the complexity and overlapping of designations, two of the following notations are considered. First, it is further assumed that the magnetic field is normalized as before, see (8), but without the corresponding " $\widetilde{\ }$ ". Second, the previously announced normalization of the coordinates also remains, e.g., $\overline{z}$, but still without an overline, that is, z.
Assuming (15)-(16), the following non-linear transmission line equations can be written:

$$\begin{aligned} \frac{\mathrm{d}}{\mathrm{d}z}\widehat{\mathbf{E}} &= -\mathrm{j}\widehat{\boldsymbol{R}}_{\mathrm{H}}\widehat{\mathbf{H}} \qquad \widehat{\boldsymbol{R}}_{\mathrm{H}} = \begin{bmatrix} 1\boldsymbol{I} & \\ & 2\boldsymbol{I} \end{bmatrix} \\ \frac{\mathrm{d}}{\mathrm{d}z}\widehat{\mathbf{H}} &= -\mathrm{j}\widehat{\boldsymbol{R}}_{\mathrm{E}}\widehat{\mathbf{E}} \qquad \widehat{\boldsymbol{R}}_{\mathrm{E}} = \begin{bmatrix} \mathrm{diag}\,(\varepsilon_{r1}) + \boldsymbol{P}_x & \mathrm{diag}\,(\chi_{21})\,\mathrm{diag}\left(\widehat{\mathbf{E}}_1^*\right) \\ \mathrm{diag}\,(\chi_{22})\,\mathrm{diag}\left(\widehat{\mathbf{E}}_1\right) & 2\mathrm{diag}\,(\varepsilon_{r2}) + \frac{1}{2}\boldsymbol{P}_x \end{bmatrix} \end{aligned} \tag{27}$$

Here $\boldsymbol{P}_x$ denotes the matrix differential operator of the 2nd order with respect to normalised z. This contains the boundary conditions on both sides of the structure, (Pregla, 2008). The matrices $\widehat{\boldsymbol{R}}_{\mathrm{E}}$ and $\widehat{\boldsymbol{R}}_{\mathrm{H}}$ are the coefficients of the NGTL equations. The material parameters ε_r and μ_r are discretized to $\widehat{\varepsilon_r}$ and $\widehat{\mu}_r$ (further represented as ε_r and μ_r, without " $\widehat{\ }$ "). The symbol "diag()", e.g., diag(ε_{r1}) or diag (χ_{21}), denotes the diagonal matrices of the discretized material parameters and of the susceptibility, accordingly. The symbol $\boldsymbol{I}$ denotes an adequate unit matrix. The tensor of the material parameters goes into the vectors $\varepsilon_{r1,r2}$. These represent the dielectric permeability in the respective cross-section of the waveguiding structure on the respective homogeneous section. The same arrangement also applies to the vectors $\chi_{21,22}$. The magnetic permeability μ_r is assumed to be equal to $\boldsymbol{I}$.
Since $\widehat{\boldsymbol{R}}_{\mathrm{E}}$ is a function of z and E_1, the wave equation has to be in terms of $\widehat{\mathbf{E}}$

$$\frac{\mathrm{d}^2\widehat{\mathbf{E}}}{\mathrm{d}z^2} + \widehat{\boldsymbol{R}}_{\mathrm{H}}\widehat{\boldsymbol{R}}_{\mathrm{E}}\widehat{\mathbf{E}} = \mathbf{0}; \quad \widehat{\boldsymbol{Q}}_{\mathrm{E}} = \widehat{\boldsymbol{R}}_{\mathrm{H}}\widehat{\boldsymbol{R}}_{\mathrm{E}} = \begin{bmatrix} \mathrm{diag}\,(\varepsilon_{r1}) + \boldsymbol{P}_x & \mathrm{diag}\,(\chi_{21})\,\mathrm{diag}\left(\widehat{\mathbf{E}}_1^*\right) \\ 2\mathrm{diag}\,(\chi_{22})\,\mathrm{diag}\left(\widehat{\mathbf{E}}_1\right) & 4\mathrm{diag}\,(\varepsilon_{r2}) + \boldsymbol{P}_x \end{bmatrix} \tag{28}$$

Neglecting the dependence of z in E_1, one obtains

$$\frac{\mathrm{d}^2\widehat{\mathbf{H}}}{\mathrm{d}z^2} + \widehat{\boldsymbol{R}}_{\mathrm{E}}\widehat{\boldsymbol{R}}_{\mathrm{H}}\widehat{\mathbf{H}} = \mathbf{0}; \quad \widehat{\boldsymbol{Q}}_{\mathrm{H}} = \widehat{\boldsymbol{R}}_{\mathrm{E}}\widehat{\boldsymbol{R}}_{\mathrm{H}} = \begin{bmatrix} \mathrm{diag}\,(\varepsilon_{r1}) + \boldsymbol{P}_x & 2\mathrm{diag}\,(\chi_{21})\,\mathrm{diag}\left(\widehat{\mathbf{E}}_1^*\right) \\ \mathrm{diag}\,(\chi_{22})\,\mathrm{diag}\left(\widehat{\mathbf{E}}_1\right) & 4\mathrm{diag}\,(\varepsilon_{r2}) + \boldsymbol{P}_x \end{bmatrix} \tag{29}$$

Transformation of the wave equation into the mode domain:

$$\begin{aligned} \widehat{\overline{\mathbf{E}}} = \widehat{\boldsymbol{T}}_{\mathrm{E}}^{-1}\widehat{\mathbf{E}} \qquad \boldsymbol{T}_{\mathrm{E}}^{-1}\widehat{\boldsymbol{Q}}_{\mathrm{E}}\boldsymbol{T}_{\mathrm{E}} = \boldsymbol{\Gamma}^2 \qquad \boldsymbol{\Gamma}^2 &= \mathrm{diag}\left(\boldsymbol{\lambda}_1^2, \boldsymbol{\lambda}_2^2\right) \\ \boldsymbol{T}_{\mathrm{E}} &= \begin{bmatrix} \boldsymbol{I} & \boldsymbol{X}_1 \\ \boldsymbol{X}_2 & \boldsymbol{I} \end{bmatrix} \end{aligned} \tag{30}$$

$$\frac{\mathrm{d}^2\widehat{\overline{\mathbf{E}}}}{\mathrm{d}z^2} + \boldsymbol{\Gamma}^2\widehat{\overline{\mathbf{E}}} = \mathbf{0} \quad \longrightarrow \quad \widehat{\overline{\mathbf{E}}} = e^{-\boldsymbol{\lambda}z}\widehat{\mathbf{A}} + e^{\boldsymbol{\lambda}z}\widehat{\mathbf{B}} \tag{31}$$

Remarks: The transformation matrix $\boldsymbol{T}_{\mathrm{E}}$ was determined from the solution of the eigenmode problem, see (30), above, in the middle. Field vectors in the transformed domain are marked with an overline, e.g., "$\overline{\mathbf{E}}_1$". The $\boldsymbol{\lambda}$ is the discretized vector of the propagation constants of the forward propagating mode $e^{-\boldsymbol{\lambda}z}\widehat{\mathbf{A}}$.

$$\overline{\mathbf{E}}_1 = e^{-\lambda_1 z}\widehat{\mathbf{A}}_1 + \boldsymbol{X}_1 e^{-\lambda_2 z}\widehat{\mathbf{A}}_2 + e^{\lambda_1 z}\widehat{\mathbf{B}}_1 + \boldsymbol{X}_1 e^{\lambda_2 z}\widehat{\mathbf{B}}_2 \tag{32}$$

$$\overline{\mathbf{E}}_2 = \boldsymbol{X}_2 e^{-\lambda_1 z}\widehat{\mathbf{A}}_1 + e^{-\lambda_2 z}\widehat{\mathbf{A}}_2 + \boldsymbol{X}_2 e^{\lambda_1 z}\widehat{\mathbf{B}}_1 + e^{\lambda_2 z}\widehat{\mathbf{B}}_2 \tag{33}$$

Phase matched case: $\lambda_1 = \lambda_2$

$$\overline{\mathbf{E}}_1 = e^{-\lambda_1 z}\left(\widehat{\mathbf{A}}_1 + \boldsymbol{X}_1\widehat{\mathbf{A}}_2\right) + e^{\lambda_1 z}\left(\widehat{\mathbf{B}}_1 + \boldsymbol{X}_1\widehat{\mathbf{B}}_2\right) \tag{34}$$

$$\overline{\mathbf{E}}_2 = e^{-\lambda_1 z}\left(\widehat{\mathbf{A}}_2 + \boldsymbol{X}_2\widehat{\mathbf{A}}_1\right) + e^{\lambda_1 z}\left(\widehat{\mathbf{B}}_2 + \boldsymbol{X}_2\widehat{\mathbf{B}}_1\right) \tag{35}$$

4 Solution of the NGTL equations

A demonstration of the general approach using a simple test structure as an example certainly cannot cover all emergent aspects. Therefore, it seems useful to discuss the most important of the aspects that the user may encounter in the case of more complex structures and more complex excitations. The topics to be treated come from the experience of earlier numerical calculations, including, e.g., (Spiller, 2022-a) and (Spiller et al, 2019).

4.1 MoL and non-linearity

The NGTL equations deal with non-linear processes. In general, the result of a calculation, i.e., an electric field distribution, - depends in principle on "itself", (27 - 29). An iterative approach to the calculation is, therefore, an option. There is a possibility to use the solutions (32-35), but also the NGTL equation (27) or the wave equations (28-29). The iterative approach means that the MoL is a part of an iterative algorithm with self-consistent, convergent solutions. In other words, a MoL-IAFT-FD solution is performed several times in succession for the entire length of the non-linear structure (interaction length of the SHG). Each next iteration uses the results calculated from the previous iteration as input data, in this case the electric fields. However, it should be ensured that the NGTL - as a non-linear differential equation - has an existing and non-singular solution to the initial value problem. According to (Hermann and Saravi, 2016), the following hypothesis can be considered.

It is assumed that Peano's existence theorem and the uniqueness theorem of Picard and Lindelöf are fulfilled, and the Picard iteration converges; see (Hermann and Saravi, 2016). Above all, this means that left and right parts of a differential equation are continuous and bounded for all points of the argument. However, the formal requirement of continuity cannot be applied directly to the discretized NGTL. The discretization himself, the possible effects of the complex values, and the possible influence of abrupt transitions in the spatial distribution of the material parameters should also be taken into account. However, a rational loosening of the formal requirement for continuity appears as helpful in this case. From practical experience, it seems less likely that instability can occur as a result of sufficiently fine discretization - as opposed to a hypothetical fully "smooth" model. Therefore, the hypothetical assumption of complete "smoothness" of the material parameters seems reasonable. This loosening of the mathematical rigor is hypothetically used as a practice-oriented tool, whereby the core statement of the mathematically strictly formulated context remains physically valid, but the limitations (discontinuity of material parameters) that are less relevant for practice are omitted. It is also known that for technological reasons, there are never perfect interfaces, but a smooth transition between two regions, (Pregla, 2008) A.1.3. Therefore such an imaginary approximation/assumption of a smooth transition is justified. A convergence of an iterative solution of the NGTL equations to a meaningful field distribution finally serves as a support for the hypothesis set out above.

4.2 On the stability and convergence of the MoL-FD

The matrix $\boldsymbol{Q}$ (or the matrices $\boldsymbol{R}_{\mathrm{E}}$ and $\boldsymbol{R}_{\mathrm{H}}$) can no longer be semidefinite depending on the spatial discretization. To assure numerical stability, additional information about the underlying concept should be used: The impedance/admittance transformation. This concept is inherently numerically stable and gives correct results for every length of section $\Delta\overline{z}$. This fact is based on a direct relation to the transmission line theory, (Chen, 2004) ch.V, which in principle provides exact analytical solutions. Also, in general, the algorithm of the impedance/admittance transformation can be understood as generalized transmission line theory, (Pregla, 2008). Thus, the GTL (and NGTL) equations, e.g., (27), show the analogy between the MoL and the well-known telegraph equations. Lines used in the MoL can also be represented as transmission lines. If one has only one mode, the recursive calculations of the impedance/admittance from the MoL reduce to to the well-known impedance/admittance transformation formulas from the transmission line theory. Hence, as shown below, the following applies: As long as individual sections (as steps of the FD) are calculated according to the rules of the transmission line theory, the impedance/admittance transformation remains for $\Delta\overline{z} \to \infty$ and $\Delta\overline{z} \to 0$ formally exact, (Pregla, 2008) (e.g., ch. 2). In other words: As long as the two-port parameters of the last section at the output of the structure are determined by short and open circuiting, - one can assume an exact impedance/admittance transformation. Of course, this accuracy relates to the formally calculated mathematical model, which does not necessarily correspond to the original, e.g., because of a too coarse discretization. It is the responsibility of the user to determine whether the discretization is sufficiently dense. If the sampling theorem is disregarded, the results will be incorrect, which, however, has to do with an incorrect application of the model. But even in this case, the impedance/admittance transformation remains formally exact and stable. If the impedance/admittance transformation is applied iteratively, the additional factors discussed in section 4 should also be taken into account.

Another numerical aspect can also be relevant for complex structures: The mathematical stiffness of the GTL and NGTL equations. In general, differential equations are mathematically “stiff” if they contain some constructs or parameters that cause rapid variations in the solutions. It is generally difficult to integrate the “stiff” equations by ordinary numerical methods. Small errors may rapidly accumulate (Bronstein et al., 2005), (Zeidler, 2004), (Curtiss and Hirschfelder, 1952), (Hairer and Wanner, 1996). With regard to the MoL, the definition of the stiffness in (Bronstein et al., 2005) appears to be suitable: An differential equation is stiff if its solutions are made up of different, strongly exponentially decreasing components. In other words, a stiffness occurs when there is a large difference in scale on the same task. It may well happen that certain strongly decreasing components hardly make a contribution to the solution but have a significant influence on the choice of the step size $\Delta\overline{z}$ so that the egg flow of the rounding error $O(1/\Delta\overline{z})$ increases very strongly, (Bronstein et al., 2005). In this case, the equation can cause a particularly high computational effort or, in extreme cases, especially with an adaptive choice of the step size, force the user to abort the calculation because of the apparent “standstill” of the calculation. In the sense, the stiff differential equations can certainly pose challenges with regard to the success of the solutions. The stiffness aspect may require a change to another method of integration of the given differential equation, e.g., to an implicit method or to the method of the other order of accuracy, more about this, see section 4.3.

The aspects of stability and stiffness in MoL-IAFT-FD, especially in the case of waveguiding structures, were discussed and tested in more detail in the paper (Spiller, 2022-a).

4.2.1 Some waveguide specifics

Spatially complex structures can exhibit complex spatial (and temporal) field distributions, which can pose an almost unforeseeable challenge for the solution of the GTL and NGTL, e.g., due to the stiffness. This applies above all to multimode waveguides with abrupt transitions in material parameters and strong permittivity contrasts. As an example, defect waveguides in photonic crystals can be mentioned, which, e.g., in the region of the defect, can show a Gaussian-shaped field in cross-section, but which are accompanied with possible side lobes with relatively abrupt rising and falling sharp peaks.

Another specific aspect occurs relatively rarely but can occasionally falsify the final result of the calculation if handled improperly. This is a change in the composition of the modes caused by certain factors during repeated calculations of the eigenvalue problem. The cause can be an already very small change of certain input parameters, e.g., a slightly different (or differently placed) longitudinal discretization. This can result in an incorrect calculation of the final result because the wrong mode is used - or the previously used mode is no longer capable of propagation under the new conditions. The background of the effect from the point of view of the numerics is the following. The number of eigenvalues computed as a solution to an eigenvalue problem is usually equal to the number of discretization points along the cross-section of the structure. The eigenvalues correspond to the eigenmodes of the waveguide. But only some of them are capable of propagation and are not evanescent (if the real part of the propagation constant is zero). If the user wants to excite one or more modes capable of propagation (such as the excitation in section 5.1), he should select these modes in the matrices appropriately and correctly distinguish them from the other eigenmodes in subsequent calculations. This can be done in two ways, either by the sequence number of the eigenvalues or by the shape of the corresponding field distribution along the cross-section of the structure (the values of this field distribution are contained in the corresponding column of the eigenvector matrix that has the same sequence number). If the calculations of the eigenvalue problem are repeated with slightly changed input parameters (e.g., with a different number of longitudinal discretization points), it can happen that the eigenmode previously assumed to be guiding now has a different sequence number - or even becomes unable to propagate. The consequences of such a “sudden” change, a reallocation, which is usually unexpected for the user - let’s call it a “mode jump” - can be fatal for the correctness of the calculation: The software routine, which is usually responsible for recognizing the guiding modes, leads now carries out further calculations with an incorrect eigenmode - or no longer finds a suitable eigenmode at all. This phenomenon also occurs in the Floquet domain: A reallocation of the Floquet modes or a loss of their ability to propagate (the criterion of propagation ability is $Re\{\boldsymbol{G}_\mathrm{F}\} = 0$, where $\boldsymbol{G}_\mathrm{F}$ is the Floquet modes phase, (Pregla, 2008)).

It is reasonable to assume that the effect of the ”mode jumps” (among other things) is closely related to the mathematical stiffness of solutions, e.g., with a coarser discretization, abrupt transitions of the material parameters, and their high contrasts.

4.3 On improving the usability: Additional methods of integrating the NGTL equations

The MoL is largely universal and is in principle able to treat almost all possible waveguiding structures in microwave technology and optics. However, the resulting generalized transmission line equations, GTL as well as

NGTL can pose different challenges to the efficiency of the finite differences - depending on the specific waveguiding structure and the excitation. For example, they can be more or less mathematically stiff, (Bronstein et al., 2005), and generally require a particularly high numerical effort or even cause the calculations to be aborted. However, these possible difficulties are by no means the disadvantage of MoL as a method, but a specific feature of the waveguiding structure investigated, linear as well as non-linear. The first possibility of improvement results from the comparison of the existing instruments of the MoL-IAFT-FD with the numerous instruments of the numerics of the ordinary differential equations (ODE). The numerics of the ODE have several method classes available for the user to choose from, e.g., one-step and multistep approaches, which in turn contain numerous methods of integrating the ODE, e.g., explicit or implicit methods of different orders of accuracy. Thus, a wide range of tasks can be calculated efficiently, as the user has multiple choices. In contrast, only two methods for the numerical integration of the ODE have been built into the MoL-IAFT-FD: linear and quadratic interpolation, so far (Pregla, 2006-a), (Pregla, 2006-b), (Pregla, 2008). It should be emphasized that standard software libraries of the ODE numerics can scarcely be used: The individual steps of the MoL-IAFT-FD are permanently linked to the steps of the fully vectorized impedance/admittance and field transformation. In this way, the possibility of choice for the user can be expanded. The main idea is that for specific complex structures, by using certain methods, the computational effort can be reduced significantly. This reduction is important for the MoL-IAFT-FD also because of the recursive character of the calculations: This reduces the probability of a cumulative accumulation of rounding errors $O(1/\Delta\overline{z})$ and thus a possible divergence of the solution, (Bronstein et al., 2005). For more details about a build-in of different one-step methods into the MoL-IAFT-FD, see (Spiller, 2022-a).

5 Numerical results and discussion

5.1 Modeling of a non-linear stripe waveguide

For demonstration, a simple stripe waveguide is considered (Fig. 1 and Fig. 2 left). This test structure was assumed as a finite length waveguide with the non-linear core. The infinitely long, structurally identical, but linear waveguides were connected to the input and output. The electric wall and Neumann boundary conditions for the normal component of the electric field were assumed on both sides, (Pregla, 2008). The first Floquet mode of the input waveguide was considered as an excitation. This was determined from the following consideration. By using the Floquets theorem, the period structure is transformed into an equivalent transmission line. In this case, the length of the non-linear part (NL) is taken as the period. Thus, the infinitely long input and output waveguides (L) are assumed to be composed of periods of the same length. This makes it possible to calculate the Floquet parameters of the infinite waveguide (L) as a periodic structure. Assume that the fundamental mode is injected with a unit amplitude, then $\widetilde{\mathbf{E}}_{\mathrm{A,f}} = [1,0,\cdots,0]^t$ is the vector of forward propagating Floquet modes. The forward propagating wave in the original domain is $\mathbf{E}_{\mathrm{A,f}} = \boldsymbol{S}_{\mathrm{E}}\widetilde{\mathbf{E}}_{\mathrm{A,f}}$, where $\boldsymbol{S}_{\mathrm{E}}$ is a Floquet-modal transformation matrix, for more details, see (Pregla, 2003) or the monograph (Pregla, 2008).

It is expected that with the material parameters used, the SHG appears as the strongest effect, (Knyazyan, Pregla, and Helfert, 2004). Therefore, only the two frequencies are considered for the sake of simplicity.

5.2 Numerical results

The hypothetical assumptions regarding the numerical stability, consistency, and convergence of the iterations appear to have been confirmed in the numerical experiment so far. In the fine discretization region, the calculations were always stable and convergent. So far, only the computation time has been found to be the upper limit of the discretization resolution. In the region of coarse discretization, an estimation of the limit of model adequacy became possible: It was found that in order to ensure reliable convergence of the MoL iterations, the FD step size Δz (with the otherwise given test parameters) should not be chosen larger than approximately $\lambda/50$. Such a limit can be considered as a limiting factor for practical applications. For example, with the length of the test structure around 20 μm and $\lambda_0 = 2\pi/(\omega\sqrt{\mu_0\varepsilon_0}) = 1550$ nm, this would mean the minimum number of discretization points along the propagation axis around 650. The number of discretization points in the cross-section of the structure has less influence on the course of the field distributions along the propagation axis but, as expected, has a significant influence on the computation time. With a smaller step length, $\Delta z < \lambda/50$, a safe and fast convergence of the solution was given in all cases of the initial conditions so that only a few iterations were necessary until the calculated distribution of the electric field visually showed no more noticeable differences in comparison to the result of the previous iteration. With this accuracy, it was hardly necessary more than 4-5 iterations.

In the paper, the calculation was performed using conventional linear and quadratic interpolation as well as several newly built-in methods. For more details about the newly built-in methods, see (Spiller, 2022-a). The best

results were obtained using the Runge-Kutta method of 4th order of accuracy: It was found, through a suitable interpolation of the solution to 20-25 times longer non-linear structures can be analyzed - with the same numerical effort - than with quadratic and linear interpolation. However, this refers to the concrete test structure and the concrete excitation, which is characterized by relatively smooth field distributions in the propagation direction.

Fig. 2 right and Fig. 3 show the spatial field distributions of the TE modes with the components Ey, Hx, and Hz. With sufficiently strong amplitudes, a secondary harmonic was effectively generated. The known effects, the SHG, as well as the bidirectional energy exchange (see below), can, in this case, serve the purpose of qualitative verification of the results.

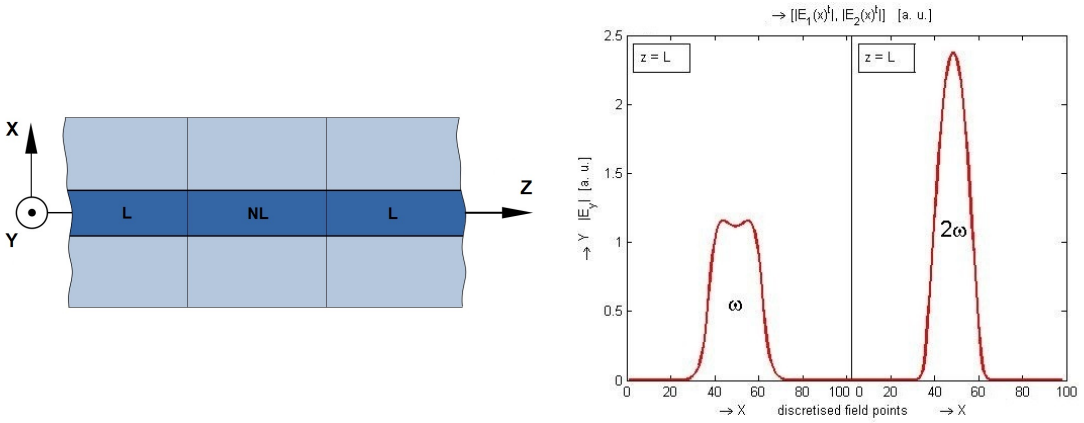

Fig. 2 Left: 2D stripe waveguide (width 29.6 μm, length 22.2 μm) with the non-linear core ($n_{core} = 2.269$, $n_{clad} = 2.254$, width 7.4 μm, $\chi_{21} = \chi_{22} = 2.0^{-11}$ m/V.) and linear waveguides connected to the input and output. $\lambda_0 = 2\pi/(\omega\sqrt{\mu_0\varepsilon_0}) = 1550$ nm. Right: Spatial field distribution of TE modes with components Ey, Hx, Hz (cross-section of spatial field distribution at the maxima of the second harmonic). The second harmonic is shown separately, as a part of a supervector of the whole field $\widehat{\mathbf{E}} = \left[\widehat{\mathbf{E}}_1^t, \widehat{\mathbf{E}}_2^t\right]^t$).

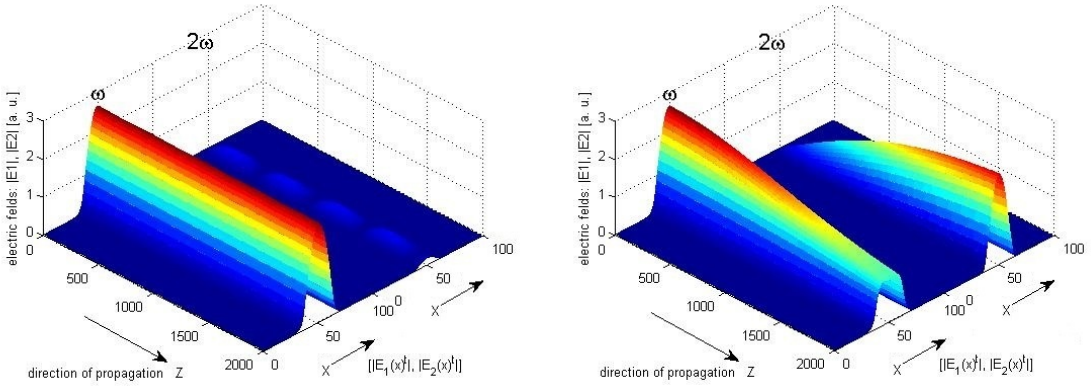

Fig. 3 Left: Phase mismatch. The second harmonic generation is not efficient. However, a certain periodicity in the weak second harmonic can already be seen. Right: Perfect phase matching. The second harmonic is effectively generated and its amplitude at the end of the calculation window exceeds the amplitude of the fundamental mode.

5.3 Modeling of the bidirectional energy exchange between harmonics

Energy exchange between the fundamental mode and the second harmonic occurs, for instance, at the second harmonic generation at sufficiently high intensities. It is periodic in nature but is accompanied by progressive deformation of the field distribution in the cross-section of the structure. The spatial period reduces with the increase of the field strength. This leads by a multi-modal non-linear waveguide to different spatial periodicities and to a jagged deformation of the original field distribution (Figs. 4 and 5).

The results are in good agreement with those in (Knyazyan, Pregla, and Helfert, 2004) and qualitatively correspond to (D'Aguanno et al., 2003-b), (D'Aguanno et al., 2003-a) and (Masoudi and Arnold, 1995).

In this numerical experiment, the interaction length was found to be a limiting factor: An interaction length had to be modeled as a whole, which would require a large number of discretization points. In this case, the choice of a suitable type of interpolation of the FD in the course of the impedance/admittance and field transformation has proven to be helpful. Through a suitable interpolation of the solution to 20-25 times longer non-linear structures can be analyzed than with quadratic and linear interpolation. Better results are obtained with one-step methods of the 4th order: Classical Runge-Kutta (RK4) and better, implicit Gauss-Runge-Kutta method (GRK4), (Hairer et al, 2007), (Bultheel and Cools, 2010), (Hairer and Wanner, 1996).

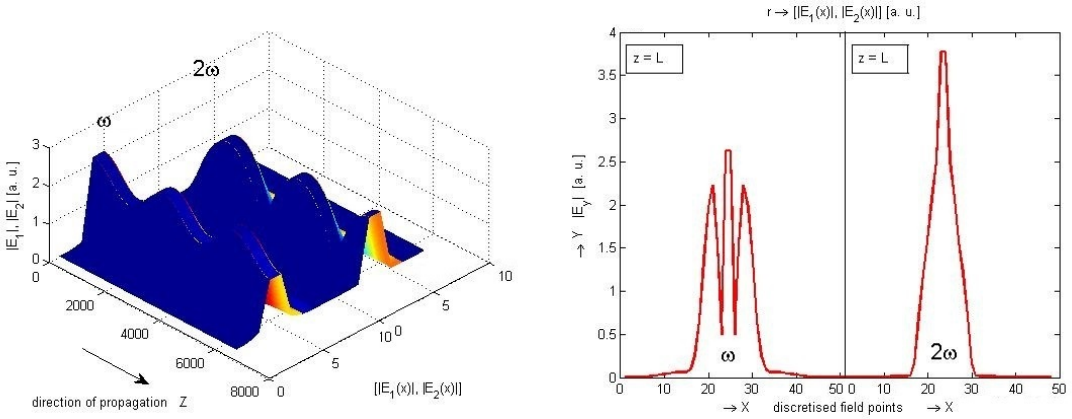

Fig. 4 Bidirectional periodic energy exchange and deformation of the original field distribution. The fundamental frequency ω and the second harmonic 2ω are shown side by side with a common longitudinal axis (interaction length). Left: The number of discretization points of the cross-section is deliberately limited. This makes the periodic nature of the effect in the longitudinal direction easier to be seen on the diagram. The amplitude of the second harmonic is at its maximum at the end of the calculation window. Right: Field distributions along the cross-section of the structure and at the end of the calculation window. The sufficiently large number of discretization points along the cross-section makes a deformation of the original field distribution visible.

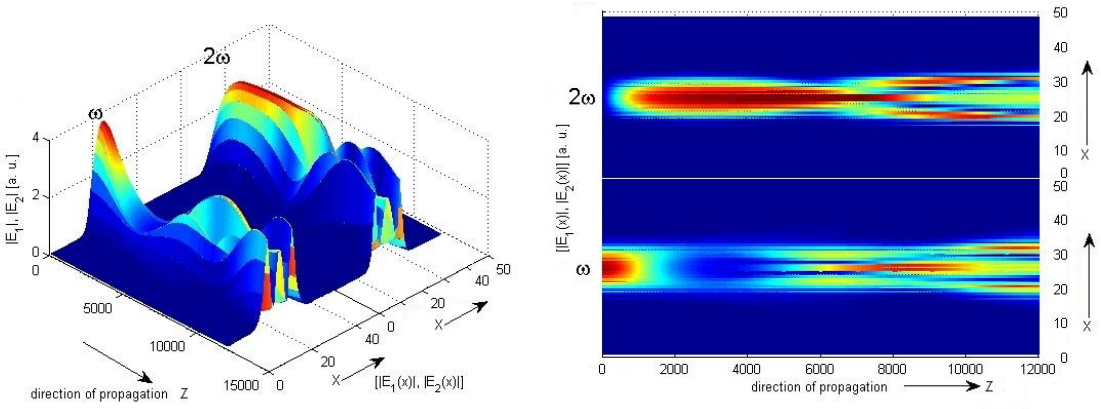

Fig. 5 Progressive deformation of the original field distribution with the interaction length. Left: The number of discretization points of the cross-section is deliberately limited. This makes the course of the field distribution in the longitudinal direction easier to see on the diagram. Right: Top view. The field distribution of the two frequency components is deformed in the course of propagation.

6 Conclusions

As an extension to the conventional linear MoL-IAFT-FD, a treatment of structures with non-linear dielectric materials is introduced. The Non-linear Generalized Transmission Line equations (NGTL) are derived from Maxwell's equations, taking into account the polarization of the medium. A 2D stripe waveguide with a non-linear core was chosen as the test structure. The Kerr non-linearity was investigated, though the general case is treatable. The Neumann boundary conditions for the normal component of the electric field were assumed on the left and right sides of the cladding. An iterative algorithm based on the impedance/admittance transformation with the field transformation obtains efficient and self-consistent solutions. This approach was used to calculate wave propagation and generation of second harmonics for various parameters.

In the fine discretization region, the calculations were always stable and convergent. So far, only the computation time has been found to be the upper limit of the discretization resolution. In the region of coarse discretization, an estimation of the limit of model adequacy became possible: It was found that in order to ensure reliable convergence of the MoL iterations, the FD step size (with the otherwise given test parameters) should not be chosen larger than a certain value, in this case, $\Delta z < \lambda/50$. Such a limit can be considered as a limiting factor for practical applications.

However, it was found, through a suitable interpolation of the solution (one-step methods Runge-Kutta of the 4th order) to 20-25 times longer non-linear structures can be analyzed than with quadratic and linear interpolation.

Bidirectional energy exchange between harmonics was found. Equality of the intensities or/and phase matching is not necessary for the effect. The spatial period of the energy exchange reduces with the increase of the field strength. This leads by a multi-modal non-linear waveguide to different spatial periodicities and to a jagged deformation of the original bell-shaped field distribution. The results were verified by comparison with similar results in the literature.

Since the selected self-consistent method remains stable and robust enough in numerical practice - in this numerical experiment, but also in, e.g., (Spiller et al, 2019), even under difficult conditions such as a pronounced mathematical stiffness, - its application can also be regarded as promising for non-linear waveguiding structures.

7 Acknowledgment

The analysis presented here was based on the excellent theory and earlier works by Univ. Prof. Dr. Reinhold Pregla. His advice is greatly appreciated. Also, I thank Dr. Stefan F. Helfert for his valuable advice and for sharing his rich experience.

A1: Determination of complex function for e_y^2

It is well known that using Euler's formulas, a time harmonic function $f = a\cos(\omega t + \phi)$ with frequency ω can also be written as $f = \frac{1}{2}(\underline{a}\mathrm{e}^{\mathrm{j}\omega t} + \underline{a}^*\mathrm{e}^{-\mathrm{j}\omega t})$ with $\underline{a} = a\mathrm{e}^{\mathrm{j}\phi}$. Let us call $a_c = \underline{a}\mathrm{e}^{\mathrm{j}\omega t}$ the complex function of f.
In this case, e_y is a sum of harmonic functions. This sum can be described as

$$e_y = \frac{1}{2}(a_c + a_c^*) \qquad a_c = E_1 e^{\mathrm{j}\omega t} + E_2 e^{\mathrm{j}2\omega t} + E_3 e^{\mathrm{j}3\omega t} + E_4 e^{\mathrm{j}4\omega t} + ... \tag{36}$$

Where a_c is now the complex function of e_y. $E_1, E_2...$ are the phasors of the harmonic functions. Now the complex function of e_y^2 is to be obtained. Using eq. (36) one obtains

$$e_y^2 = \frac{1}{4}(a_c^2 + a_c^{*2} + 2a_c a_c^*) = \frac{1}{2}(\frac{a_c^2 + a_c^{*2}}{2} + b_c + b_c^* + C) = \frac{1}{2}(E_{yc}^q + E_{yc}^{q*} + C) \tag{37}$$

Where $a_c a_c^* = b_c + b_c^* + C$ and E_{yc}^q is the complex function of e_y^2. As seen E_{yc}^q is equal to $E_{yc}^q = \frac{1}{2}a_c^2 + b_c$. For the parts a_c^2 one obtains

$$\begin{aligned} a_c^2 = {} & E_1^2 e^{2\mathrm{j}\omega t} + 2E_1E_2 e^{3\mathrm{j}\omega t} + \left(E_2^2 + 2E_1E_3\right) e^{4\mathrm{j}\omega t} + \\ & 2\left(E_1E_4 + E_2E_3\right) e^{5\mathrm{j}\omega t} + \left(E_3^2 + 2E_1E_5 + 2E_2E_4\right) e^{6\mathrm{j}\omega t} + \\ & 2\left(E_1E_6 + E_2E_5 + E_3E_4\right) e^{7\mathrm{j}\omega t} + ... \end{aligned} \tag{38}$$

and for the product $a_c a_c^*$

$$\begin{aligned} a_c a_c^* = & E_1 E_1^* + E_2 E_2^* + E_3 E_3^* + E_4 E_4^* + ... \\ & + (E_2 E_1^* + E_3 E_2^* + E_4 E_3^* + ...)\, e^{\mathrm{j}\omega t} + (E_1 E_2^* + E_2 E_3^* + ...)\, e^{-\mathrm{j}\omega t} \\ & + (E_3 E_1^* + E_4 E_2^* + E_5 E_3^* + ...)\, e^{2\mathrm{j}\omega t} + (E_3^* E_1 + E_4^* E_2 + ...)\, e^{-2\mathrm{j}\omega t} \\ & + (E_4 E_1^* + E_5 E_2^* + E_6 E_3^* + ...)\, e^{3\mathrm{j}\omega t} + (E_4^* E_1 + E_5^* E_2 + ...)\, e^{-3\mathrm{j}\omega t} \\ & + ... \end{aligned} \tag{39}$$

The first row is equal to a constant value which vanishes after differentiation with respect to time. It is evident that the first parts of the other rows correspond to b_c and the second part to b_c^*. Therefore, the complex function E_{yc}^q is now given by

$$\begin{aligned} E_{yc}^q = & \frac{1}{2} a_c^2 + b_c = E_{y1}^q e^{\mathrm{j}\omega t} + E_{y2}^q e^{\mathrm{j}2\omega t} + E_{y3}^q e^{\mathrm{j}3\omega t} + ... \\ & = e^{\mathrm{j}\omega t} (E_1^* E_2 + E_2^* E_3 + E_3^* E_4 + ...) \\ & + e^{\mathrm{j}2\omega t} \left(\frac{1}{2} E_1^2 + E_1^* E_3 + E_2^* E_4 + E_3^* E_5 + ... \right) \\ & + e^{\mathrm{j}3\omega t} (E_1 E_2 + E_1^* E_4 + E_2^* E_5 + E_3^* E_6 + ...) \\ & + e^{\mathrm{j}4\omega t} \left(\frac{1}{2} E_2^2 + E_1 E_3 + E_1^* E_5 + E_2^* E_6 + E_3^* E_7 + ... \right) \\ & + e^{\mathrm{j}5\omega t} (E_1 E_4 + E_2 E_3 + E_1^* E_6 + E_2^* E_7 + E_3^* E_8 + ...) \\ & + ... \end{aligned} \tag{40}$$

Neglect all harmonic functions with frequencies larger than 2ω one obtains the following expression for the case of second harmonic generation

$$E_{yc}^2 = E_1^* E_2 e^{\mathrm{j}\omega t} + \frac{1}{2} E_1^2 e^{\mathrm{j}2\omega t} \tag{41}$$

References

Agrawal G P (2007) Nonlinear Fiber Optics. 4th ed. Academic Press, Boston, 2007.

D'Aguanno G and Centini M and Scalora M and Sibilia C and Bertolotti M and Bloemer M J and Bowden C M (2003) Energy exchange properties during second-harmonic generation in finite one-dimensional photonic band-gap structures with deep gratings, APS, Physical Review E, vol. 67, no. 1, 016606, 2003.

D'Aguanno G and Centini M and Scalora M and Sibilia C and Bertolotti M and Bloemer M J and Bowden C M (2003) Energy exchange properties during second harmonic generation in finite photonic band gap structures, IEEE, 2003 Conference on Lasers and Electro-Optics Europe (CLEO/Europe 2003)(IEEE Cat. No. 03TH8666), p. 251, 2003.

Boyd R W (2020) Nonlinear Optics, Academic Press, 2020.

Boyd R W and Fischer G L (2001) Nonlinear optical Materials, Encyclopedia of Materials, Science and Technology, pp. 6237–6244, 2001.

Bronstein i N, Semendjaew K A, Musiol G and Mühlig H, (2005) Taschenbuch der Mathematik, Verlag Harri Deutsch, 2005.

Bultheel A and Cools R (2010) The Birth of Numerical Analysis, World Scientific, 2010.

Chen W K (2004) The electrical engineering handbook, Elsevier, 2004.

Curtiss C F and Hirschfelder J O. (1952) Integration of Stiff Equations. Proc. Nat. Acad. Sci. of the U S. A. 38:235–243, 1952.

Gómez-Ullate D and Lombardo S and Mañas M and Mazzocco M and Nijhoff F and Sommacal M (2010) Integrability and nonlinear phenomena, IOP Publishing, Journal of Physics A: Mathematical and Theoretical, vol. 43, no. 43, pp. 430301, 2010.

Hairer E, Nørsett S P and Wanner G (1993) Solving ordinary differential equations. 1, Nonstiff problems. Springer Verlag, 1993.

Hairer E and Wanner G (1996) Solving Ordinary Differential Equations II: Stiff and Differential-Algebraic Problems, Springer 2, 1996.

Helfert S F, Barcz A and Pregla R (2003) Three-dimensional vectorial analysis of waveguide structures with the method of lines. Springer, Optical and quantum electronics, vol. 35, nr. 4, pp. 381–394, 2003.

Helfert S F A and Pregla R (2002) The method of lines: a versatile tool for the analysis of waveguide structures. Electromagnetics, vol. 22, pp. 615–637, 2002. Invited paper for the special issue on ”Optical wave propagation in guiding structures”.

Helfert S F A and Pregla R (1996) Finite Difference Expressions for Arbitrarily Positioned Dielectric Steps in Waveguide Structures, J. Lightwave Technol., vol. 14, no. 10, pp. 2414–2421, Oct. 1996.

Hermann M and Saravi M (2016) Nonlinear ordinary differential equations, Springer India, doi, vol. 10, pp. 978–981, 2016.

Jamid H A and Akram M N (2002) Analysis of deep waveguide gratings: An efficient cascading and doubling algorithm in the method of lines framework. IEEE, Journal of lightwave technology, vol. 20, no. 7, pp. 1204, 2002.

Knyazyan T, Pregla R, Helfert S (2004) Method of lines for modelling second order nonlinear phenomena in planar optical waveguides. The 12th International Workshop on Optical Waveguide Theory and Numerical Modelling, Ghent, Belgium, March 22-23, 2004.

Masoudi H M and Arnold J M (1995) Modeling second-order nonlinear effects in optical waveguides using a parallel-processing beam propagation method. IEEE journal of quantum electronics, vol. 31, no. 12, pp. 2107–2113, 1995.

Pregla R and Helfert S F (2002) Modeling of Microwave devices with the method of lines. Recent Research developments in Microwave Theory & Techniques, pp. 145–196, Research Signpost, Kerala, India, 2002.

Pregla R (2006) Analysis of Microvawe Structures by Combination of the Method of Lines and Finite Differences. In: MICON (08.-09.04.2006, Crasow, Poland), 2006.

Pregla R (2006) Modeling of optical waveguides and devices by combination of the method of lines and finite differences of second order accuracy. In: Optical and Quantum Electronics, 38 pp. 3–17, 2006.

Pregla R (2003) Efficient Modeling of Periodic Structures. AEU, vol. 57, pp. 185–189, 2003.

Pregla R (2008) Analysis of Electromagnetic Fields and Waves - The Method of Lines. Wiley & Sons, Chichester, UK, 2008.

Saleh B and Teich M (2007) Fundamentals of Photonics. John Wiley and Sons, Inc., 2007.

Samarski A A (1986) Introducción a los Métodos Numéricos, Mir, 1986.

Spiller W, Helfert S F and Jahns J (2019) The numerical investigation of colliding optical solitons as an all-optical-gate using the method of Lines. Springer, Optical and Quantum Electronics, vol. 51, nr. 5, pp. 1–22, 2019.

Spiller W (2022) An enhancement of instruments for solution of general transmission line equations with method of lines, impedance-/admittance and field transformation in combination with finite differences, Research-Square, to be published.

Zeidler E (2004) Oxford Users’ Guide to Mathematics. Oxford University Press, 2004.